




Fluctuating entropy production on the coarse-grained level: Inference and localization of irreversibility

Julius Degünther ^{*}, Jann van der Meer ^{*}, and Udo Seifert 

II. Institut für Theoretische Physik, Universität Stuttgart, 70550 Stuttgart, Germany



(Received 13 September 2023; accepted 12 March 2024; published 16 May 2024)

Stochastic thermodynamics provides the framework to analyze thermodynamic laws and quantities along individual trajectories of small but fully observable systems. If the observable level fails to capture all relevant degrees of freedom, some form of effective, coarse-grained dynamics naturally emerges for which the principles of stochastic thermodynamics generally cease to be applicable straightforwardly. Our work unifies the notion of entropy production along an individual trajectory with that of a coarse-grained dynamics by establishing a framework based on snippets and Markovian events as fundamental building blocks. A key asset of a trajectory-based fluctuating entropy production is the ability to localize individual contributions to the total entropy production in time and space. As an illustration and potential application for inference we introduce a method for the detection of hidden driving. The framework applies equally to even and odd variables and, therefore, includes the peculiar case of entropy production in underdamped Langevin dynamics.

DOI: [10.1103/PhysRevResearch.6.023175](https://doi.org/10.1103/PhysRevResearch.6.023175)

I. INTRODUCTION

How can we apply the principles of stochastic thermodynamics to effective descriptions? Originally, stochastic thermodynamics emerged as a framework to identify and formulate thermodynamic laws for small-scale systems coupled to the environment via, e.g., random thermal fluctuations and driving forces [1,2]. As the dynamics itself and, consequently, associated thermodynamic quantities like heat, work, or entropy become inherently stochastic, the notion of a “system” only makes sense if there is a meaningful, “clean” separation from the environment. More specifically, a meaningful notion of energy or entropy requires a notion of “thermodynamic consistency” when implementing external effects into the stochastic dynamics of the system.

Thus, if such a system can be identified, e.g., in the form of a Langevin equation or Markovian dynamics on a discrete set of states, the framework of stochastic thermodynamics provides far-reaching, universal relations like, e.g., the Jarzynski equality and its generalizations [3–5], different formulations of fluctuation theorems [6–10], the Hatano-Sasa relation [11], and the Harada-Sasa relation [12], many of which have been realized experimentally, as reviewed in Ref. [13].

These results are formulated for a complete system in the sense that the stochastic dynamics gives rise to trajectories that include all relevant degrees of freedom. With complex

real-world systems in mind, we can ask what remains if we are unable to observe the full system or, even worse, if a clear distinction between system and environment cannot be made based on the available data. Such questions have seen growing interest in recent research, leading to a point where the study of partially accessible information might be regarded as an emerging pillar of stochastic thermodynamics in its own right.

Up to now, the study of stochastic thermodynamics of partial information contains two mostly disjointed aspects. Existing methods of thermodynamic inference [14] mainly focus on extracting or deducing particular averaged quantities based on thermodynamic relations and limited access to observables. However, a partially accessible system features its own effective dynamical laws, which emerge as a projection of the underlying dynamics. Thus, inference techniques formulated on such a dynamical level should be able to provide thermodynamic bounds on a fluctuating level beyond simple averages.

In contrast, thermodynamic inference employs a variety of methods primarily aiming at the estimation of mean entropy production. Most prominently, various formulations and generalizations of the thermodynamic uncertainty relation [15–17] provide bounds on the minimal thermodynamic cost to achieve a certain precision of, e.g., a current. Furthermore, lower bounds on entropy production can also be based on an identification as a Kullback-Leibler divergence [18–24], the speed at which the system evolves in time [25,26], stopping times [27], waiting times [28], and counting events [29]. Novel recent approaches include dynamical correlations into entropy estimation techniques by relating entropy production to the asymmetry of cross-correlations of accessible observables [30–32], their power spectral density [33], correlation times [34], or, more technically, the spectrum associated with the dynamics [35]. Beyond estimating the average value of entropy production, inference techniques for the topology of

^{*}These authors contributed equally to this work.

the underlying system [36,37] and its driving affinities [30,38] have also been proposed.

The dynamics of coarse-grained systems received much attention in earlier works on stochastic thermodynamics, usually in the context of state lumping [39,40]. More recently, a gradual paradigm shift in the conception of coarse graining challenges established paradigms [41,42]. To fully understand real-world scenarios it seems indispensable to find descriptions for dynamics on the coarse-grained level, with recent approaches including milestone [43,44] or semi-Markov dynamics [38].

The present work unifies the notion of entropy production along a single trajectory with that of coarse-grained dynamics. We establish a framework that allows us to identify entropy production along individual trajectories that retains meaning on the levels of both the underlying system and the coarse-grained, observable one, even if the coarse-grained dynamics does not obey simple rules like a master or Langevin equation. The concept of fluctuating entropy production for individual, coarse-grained paths comes along with the ability to localize individual contributions to the total entropy production in time and space within the coarse-grained description. This new aspect enables the inference of more detailed information far beyond the average total entropy production of a system. In this sense, the present work extends and complements the conceptually related Ref. [22], which derives a general estimator for the mean entropy production. From a practical viewpoint, we demonstrate that the ability to attribute irreversibility to specific events or transitions between these provides access to complex settings like the localization of entropy production in the absence of any visible states as well as the qualitative and quantitative detection of irreversibility in hidden parts of the system.

The paper is structured as follows. In Sec. II, we start with an outline of our main results and the setup under consideration. We then present our theoretical framework by introducing the two crucial concepts through which the identification of the fluctuating entropy production becomes possible. Based on this framework, we derive methods to detect and quantify hidden driving by localizing entropy production and estimating affinities of hidden cycles, as described in Sec. III. In Sec. IV, we discuss the intricacies of entropy production in the presence of odd variables. In particular, we show that the present identification of entropy production is compatible with odd variables that occur in underdamped Langevin dynamics and transition-based coarse graining. We conclude in Sec. V.

II. MAIN RESULTS AND FRAMEWORK

A. Illustration of the main concept

In real-world scenarios we commonly encounter systems for which a description that can be considered “complete” or “fundamental” in an appropriate sense would be highly complex. Thus, simplified descriptions for such systems that capture its key characteristics are indispensable. In this context, Markov networks have become one of the predominant paradigms for which the entire well-established framework of stochastic thermodynamics is available. A description based

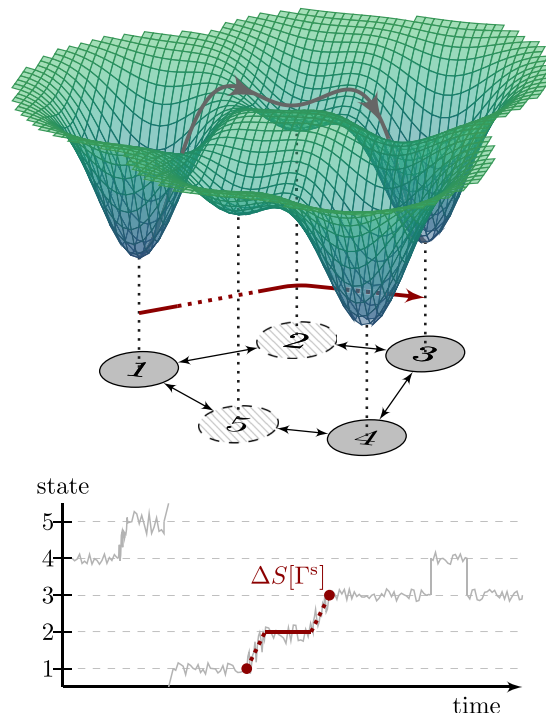


FIG. 1. Projection of a continuous energy landscape onto a set of five discrete states. States 2 and 5 cannot be modeled as Markov states due to their shallow local minima. For transitions involving these states, there is no clear timescale separation as illustrated by the time series in the lower part. The curve in the landscape in the upper part shows a section of an individual microscopic trajectory. In the lower part we show this section and how it is embedded into a longer trajectory. In both parts, the red lines depict the corresponding section of the coarse-grained trajectory. We assign an entropy production to such sections that are both localized in time and space. This identification of entropy productions retains physical significance even on the coarse-grained level.

on Markov networks typically requires the presence of clear timescale separations to separate system and environment. However, the nature of the underlying system or insufficient observational data may jeopardize such a clear timescale separation. Our framework is designed for descriptions that lack this clear separation.

These aspects are qualitatively illustrated in Fig. 1. The energy landscape gives rise to five observable discrete states. The local minima at states 1, 3, and 4 are sufficiently deep to justify a description as Markov states, in contrast to the shallow minima of states 2 and 5. The red line shows an exemplary trajectory, which, on the observable level, reads $1 \rightarrow 2 \rightarrow 3$. We will show how to identify a fluctuating entropy production for such trajectories that include non-Markovian observables like, in this case, state 2. This coarse-grained entropy production obeys several consistency conditions and provides an estimator for the entropy production on the fundamental level.

The ability to localize entropy production in this example translates into the ability to discern contributions to the total entropy production of, e.g., trajectory sections of the type $1 \rightarrow 2 \rightarrow 3$ from the remaining ones as indicated in the lower part of Fig. 1. Similarly, it is possible to localize the entropy

production in time. Depending on the application, one might be interested in the contributions that arise from, e.g., particularly fast trajectories.

B. General setup

We consider a stochastic physical system whose microscopic trajectories γ are drawn according to some path weight $\mathcal{P}[\gamma]$. For example, if the time evolution $\gamma(t)$ obeys a Langevin or master equation, a corresponding path weight is known [1]. We now assume that an observer can only measure particular observables, which give rise to a coarse-grained trajectory, rather than accessing this underlying level of description directly.

The probability to observe a particular coarse-grained trajectory Γ is encoded in its path weight $\mathcal{P}[\Gamma]$ and uniquely determined by the microscopic path weight $\mathcal{P}[\gamma]$ and the coarse graining $\gamma \mapsto \Gamma$. Similarly, the probability to observe the corresponding time-reversed trajectory $\tilde{\Gamma}$ is determined by $\tilde{\gamma}$. Thus, calculating $\mathcal{P}[\tilde{\Gamma}]$ either requires knowing the microscopic time-reversal operation $\gamma \mapsto \tilde{\gamma}$ or knowing how the coarse-grained observables behave under time reversal. Reversing the coarse-grained trajectory Γ generally not only means to read Γ backwards, but also to modify its observables. This is the case when measuring, e.g., momenta or transitions. Put informally, a physical time-reversal operation not only requires “playing the movie backwards” but also “knowing what the movie shows,” i.e., understanding the physical meaning of the model and the observables. This knowledge about the observables determines their time reversal.

C. Markovian events

We define Markovian events as particular observables whose detection implies conditional independence between past and future time evolution of γ . Such an instantaneous event determines the underlying state of the system from a dynamical point of view. We formalize the defining property for a Markovian event \mathcal{I} as

$$\mathcal{P}[\gamma_+|\mathcal{I}, \gamma_-] = \mathcal{P}[\gamma_+|\mathcal{I}] \tag{1}$$

for any trajectory $\gamma_- \rightarrow \mathcal{I} \rightarrow \gamma_+$, which contains \mathcal{I} between its past and future time evolution γ_- and γ_+ , respectively. Importantly, these events are Markovian on the microscopic level.

Generally, the state of the system is fully described by including both a suitable observation I and the absolute time τ at which it occurs. Therefore, a Markovian event takes the form of a tuple,

$$\mathcal{I} \equiv (I, \tau). \tag{2}$$

Suitable observations I are, for example, registering a transition or the current state of the system in the case of master equation dynamics on a Markov network. In the continuous case, measuring the position or both position and momentum qualifies as a Markovian event for overdamped and underdamped Langevin dynamics, respectively. We denote Markovian events by script letters $\mathcal{I}, \mathcal{J}, \dots$ to emphasize an explicit time dependence. If a Markovian event occurs at time τ , we denote the probability that this event is \mathcal{I} by $P(\mathcal{I})$. Note

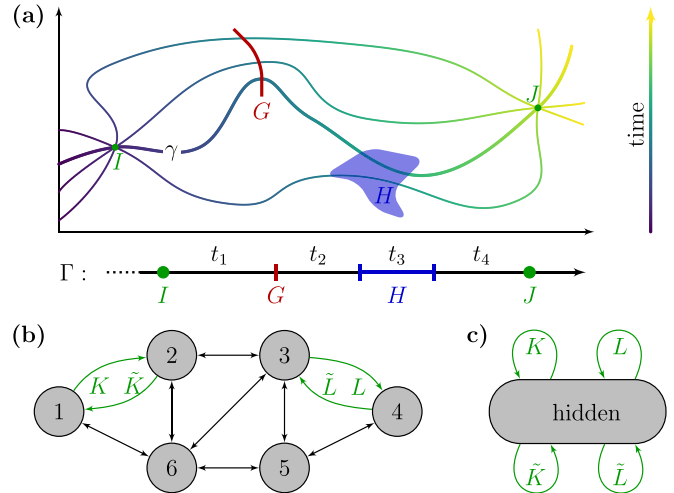


FIG. 2. (a) Qualitative illustration of Markovian events, non-Markovian events, and snippets. The upper part shows four microscopic trajectories in a two-dimensional configuration space. The elapsed time in this system is encoded in the color gradient along each trajectory. In the lower part, we show the coarse-grained trajectory Γ corresponding to the microscopic one denoted by γ . (b) Markov network with six states. We assume that only the transitions K and L and their reversed \tilde{K} and \tilde{L} can be observed. (c) Coarse-grained description of the network shown in (a).

that in stationary systems the information about the absolute time τ is not required, which makes I itself the Markovian event. In particular, $P(I)$ then becomes the probability that a registered event in the stationary state corresponds to observation I .

A coarse-grained trajectory may contain additional data besides Markovian events. We summarize such observables under the (potentially multidimensional) symbol \mathcal{O}_k , which includes any additional non-Markovian observables between the Markovian events \mathcal{I}_{k-1} and \mathcal{I}_k whose behavior under time reversal is known, in accordance with the discussion in Sec. II B. Thus, we write a coarse-grained trajectory as

$$\Gamma = (\mathcal{I}_0 \xrightarrow{t_1, \mathcal{O}_1} \mathcal{I}_1 \xrightarrow{t_2, \mathcal{O}_2} \dots \xrightarrow{t_n, \mathcal{O}_n} \mathcal{I}_n), \tag{3}$$

where the waiting times t_k between the Markovian events \mathcal{I}_{k-1} and \mathcal{I}_k are explicitly highlighted. We emphasize that the coarse-grained trajectory Γ is initialized and terminated with a Markovian event. The additional data summarized under \mathcal{O}_k may contain variables that take continuous values like, e.g., the precise time we register a transition in a Markov network if we lack the knowledge which microscopic states this transition connects or if we resolve some but not all position (and/or momentum, if applicable) coordinates of a Langevin particle. It is also possible to include variables that take discrete values like the binary information whether a lumped state has been visited or not, as we will illustrate in an explicit example in Sec. III B.

We illustrate these different types of events in Fig. 2(a). The upper part shows four different microscopic trajectories in a two-dimensional configuration space. In this setup of incomplete information, we are limited to certain observations here denoted by I, J, H , and G as well as the elapsed time in

the system indicated by the color gradient of the trajectories, which leads to coarse-grained trajectories like the one shown in the lower part of Fig. 2(a). In this case, a Markovian event is the observation of I or J in conjunction with the corresponding absolute time since these entirely determine the current microscopic configuration of the system. The non-Markovian events G and H provide additional information about the microscopic path without fully resolving the microscopic state of the system.

D. Snippets

Given a coarse-grained trajectory (3), we define a snippet [22] Γ^s as a section of Γ , which starts with a Markovian event \mathcal{I} and ends with the subsequent Markovian event \mathcal{J} :

$$\begin{aligned} \Gamma^s : \mathcal{I} &\xrightarrow{t, \mathcal{O}} \mathcal{J} \\ (I, \tau) &\xrightarrow{\mathcal{O}} (J, \tau + t). \end{aligned} \quad (4)$$

In Fig. 2(a), we illustrate a snippet that starts and ends with the Markovian events \mathcal{I} and \mathcal{J} , respectively, and additionally contains the observations G and H along with the waiting times t_1, t_2, t_3 , and t_4 . In general, any coarse-grained trajectory Γ comprises several of such snippets. In particular, the path weight associated with the trajectory (3) factorizes into contributions from the individual snippets,

$$\mathcal{P}[\Gamma|\mathcal{I}_0] = \mathcal{P}[\Gamma_1^s|\mathcal{I}_0] \cdots \mathcal{P}[\Gamma_n^s|\mathcal{I}_{n-1}], \quad (5)$$

where Γ_i^s denotes the snippet between the Markovian events \mathcal{I}_{i-1} and \mathcal{I}_i .

In the case of stationary systems, an alternative notation for the path weight of a snippet (4) is given by

$$\psi_{\mathcal{I} \rightarrow \mathcal{J}}(t; \mathcal{O}) \equiv \mathcal{P}[\Gamma^s|\mathcal{I}], \quad (6)$$

which concisely presents all relevant information, since the absolute time τ is not required so that the Markovian events are just the observations, i.e., $\mathcal{I} = I$ and $\mathcal{J} = J$. Additionally, it highlights the waiting time characteristics of the path weights $\mathcal{P}[\Gamma^s|\mathcal{I}]$. Although useful for explicit calculations, this notation easily appears overloaded if the system evolves in time. Therefore, we exclusively use it for systems in a stationary state.

E. Entropy production

Markovian events and snippets are the fundamental building blocks that allow us to extend the concept of a fluctuating entropy production to the coarse-grained level. For a system with constant driving but not necessarily in a stationary state, we identify

$$\Delta S[\Gamma^s] = \ln \frac{P(\mathcal{I})\mathcal{P}[\Gamma^s|\mathcal{I}]}{P(\mathcal{J})\mathcal{P}[\tilde{\Gamma}^s|\tilde{\mathcal{J}}]} \quad (7)$$

as the entropy production of a snippet Γ^s . It generally depends on the initial and final events \mathcal{I} and \mathcal{J} as well as the duration t and the remaining observables \mathcal{O} . For this identification to be physically meaningful, we assume that the entropy production on the microscopic level $\Delta s[\gamma]$ is of the form that is further detailed below in Sec. II G. This assumption is justified for virtually all classes of systems that are described in the

general setup and for which a physical entropy production is of interest, such as Markov networks or Langevin dynamics. For Eq. (7), we do not need to discern between descriptions based on observables that are even under time reversal, such as state-based descriptions or overdamped Langevin dynamics, and descriptions based on observables that are odd under time reversal, such as transition-based descriptions or underdamped Langevin dynamics. In Sec. IV we provide further details regarding the peculiar odd observables, which provide further support for the identification (7).

The following properties embed this notion of entropy production along the coarse-grained trajectory (7) into the framework of stochastic thermodynamics. First, it is additive in the sense that the entropy production of a coarse-grained trajectory (3) is the sum of the entropy production of its snippets,

$$\Delta S[\Gamma] = \ln \left(\frac{P(\mathcal{I}_0)\mathcal{P}[\Gamma|\mathcal{I}_0]}{P(\mathcal{I}_n)\mathcal{P}[\tilde{\Gamma}|\mathcal{I}_n]} \right) = \sum_{i=1}^n \Delta S[\Gamma_i^s], \quad (8)$$

where we use Eqs. (5) and (7). Entropy production has to be assigned in a way to avoid overcounting at the start and end points, respectively. In Eq. (7), the entropy production of a snippet includes its initial Markovian event but not the concluding one, which becomes more apparent when rewriting the entropy production (7) as

$$\Delta S[\Gamma^s] = \ln \frac{\mathcal{P}^{\text{cf}}[\Gamma^s|\mathcal{J}]}{\mathcal{P}[\tilde{\Gamma}^s|\tilde{\mathcal{J}}]}, \quad (9)$$

where the path weights exclude \mathcal{J} and $\tilde{\mathcal{J}}$, respectively. The superscript ‘‘cf’’ indicates that the path weight $\mathcal{P}^{\text{cf}}[\Gamma^s|\mathcal{J}]$ is conditioned on the final event of the trajectory snippet rather than the initial one.

Second, the coarse-grained entropy production ΔS and the microscopic entropy production Δs are linked by the exact relation

$$e^{-\Delta S[\Gamma]} = \langle e^{-\Delta s}[\Gamma] \rangle, \quad (10)$$

as we show in Appendix A. The conditional mean $\langle \cdot | \Gamma \rangle$ denotes an average over all microscopic trajectories that are mapped to Γ under coarse graining. In particular, this implies $\Delta S[\Gamma] = 0$ if the underlying system is in equilibrium, where $\Delta s[\gamma] = 0$ holds for all γ . Furthermore, equality (10) implies the thermodynamic consistency condition

$$\Delta S[\Gamma] \leq \langle \Delta s[\Gamma] \rangle \quad (11)$$

for the coarse-grained entropy production. While equality (10) might typically be of a more theoretical rather than practical significance due to the statistically demanding nature of the mean [3], inequality (11) will prove to be a useful and versatile tool for thermodynamic inference. In particular, it enables us to estimate entropy production localized in space and time. As a side note, inequality (11) directly implies the estimator

$$\langle \Delta S \rangle \leq \langle \Delta s \rangle \quad (12)$$

for the mean total entropy production of the system, which recovers the result in Ref. [22] for the mean total entropy production rate following a different reasoning. In contrast to Ref. [22], we *a priori* do not assume that the coarse-grained entropy production is related to the logarithmic ratio of path

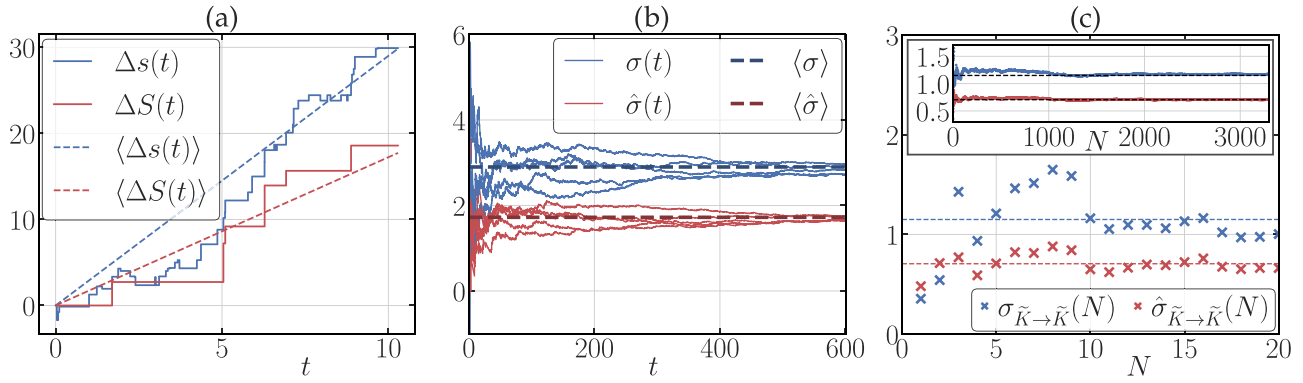


FIG. 3. Entropy production as a fluctuating quantity on the coarse-grained level in the steady state. All data are generated using the network shown in Fig. 2(b). The rates used for simulations and further numerical details are provided in Appendix D. Blue lines and markers indicate quantities on the microscopic level, whereas the coarse-grained level is denoted with red lines and markers. (a) The solid lines show the change in total entropy as a function of time along an individual trajectory both on the microscopic and the coarse-grained level. The dashed lines show the corresponding expectation values. (b) The solid lines show the total entropy production rate as a function of time along an individual trajectory for a sample of five trajectories on the microscopic and the coarse-grained level. The darker dashed lines show the corresponding expectation values $\langle\sigma\rangle \simeq 2.9$ and $\langle\hat{\sigma}\rangle \simeq 1.7$. (c) The markers show the localized entropy production both on the microscopic and the coarse-grained level as defined in Eqs. (14) and (15), respectively. The statistics is obtained by considering a long trajectory in which occasionally snippets occur that start and end with the transition $\tilde{K} = (21)$ [see Fig. 2(b)]. As shown in the inset, the entropy production rates $\sigma_{\tilde{K} \rightarrow \tilde{K}}(N) \rightarrow 1.15$ and $\hat{\sigma}_{\tilde{K} \rightarrow \tilde{K}}(N) \rightarrow 0.70$ converge towards their expectation values as $N \rightarrow \infty$, i.e., for a sufficiently large number of occurrences. An inequality of the form of Eq. (11) that involves a conditional average does not hold directly for the blue dots, which depict individual microscopic realizations of a snippet $\tilde{K} \rightarrow \tilde{K}$.

weights on the coarse-grained level. Instead, the reasoning is based on the microscopic level on which a meaningful entropy production on the trajectory level can be assumed. Therefore, a consistency condition of the form of Eq. (10) requires Markovian events on the microscopic level, whereas the derivation of a single bound on the mean values of the form of Eq. (12) only requires Markovian events on the coarse-grained level in Ref. [22].

Third, the coarse-grained entropy production $\Delta S[\Gamma]$ extends the notion of a fluctuating entropy production to the coarse-grained level. One of the major achievements of stochastic thermodynamics has been to identify entropy production as a fluctuating quantity along individual trajectories [45], which Eq. (7) generalizes beyond microscopic trajectories. Conceptually, it is a key novelty to have a coarse-grained entropy production, which is endowed with physical meaning beyond its expectation value.

F. Fluctuating entropy production on the coarse-grained level

We illustrate key aspects of the fluctuating entropy production using the concrete example shown in Fig. 2(b), a six-state Markov network in its nonequilibrium steady state. We assume that in the coarse-grained description only transitions $K = (12)$ and $L = (34)$ as well as their time-reversed counterparts $\tilde{K} = (21)$ and $\tilde{L} = (43)$ can be observed, which gives rise to the coarse-grained network shown in Fig. 2(c). In this system, the observable transitions serve as Markovian events and the resulting snippets contain no additional non-Markovian events. For the following examples we generate the coarse-grained trajectories by simulating the microscopic ones, to which the coarse-graining is applied subsequently. This procedure is in accordance with real-world scenarios in the sense that the actual dynamics takes place on the

microscopic level, but only data on the coarse-grained level are available to the observer. Since a snippet necessarily starts with a Markovian event we have to discard the initial section of a microscopic trajectory prior to the first Markovian event to ensure a simultaneous initialization of the coarse-grained and microscopic process. Analogously, the microscopic trajectories need to end with a Markovian event.

The previously exclusively microscopic concept of a fluctuating entropy production can now be applied to a coarse-grained description. We denote the total entropy production up to time t on the microscopic level as $\Delta s(t)$ and, analogously, on the coarse-grained level as $\Delta S(t)$. These quantities relate to the corresponding entropy production rates via

$$\sigma(t) \equiv \Delta s(t)/t \quad \text{and} \quad \hat{\sigma}(t) \equiv \Delta S(t)/t, \quad (13)$$

respectively. For some trajectories of the system from Fig. 2(b), the total entropy production and the total entropy production rate along individual fluctuating trajectories on both levels is shown in Figs. 3(a) and 3(b), respectively. In the coarse-grained description, the rate of jumps is lower due to the lower rate of events that contribute to the entropy production. The respective expectation values fulfill inequality (12). The rate of coarse-grained entropy production converges towards its expectation value for each trajectory Γ individually in the long-time limit, similarly to its microscopic counterpart.

The localized entropy production exhibits a similar fluctuating behavior. We define the entropy production rate after N realizations $\{\gamma_1, \dots, \gamma_N\}$ of trajectories that all start in I and end in J as

$$\sigma_{I \rightarrow J}(N) \equiv \frac{1}{T(N)} \sum_{i=1}^N \Delta s[\gamma_i] \quad (14)$$

and similarly its coarse-grained analog that is defined through the corresponding snippets $\{\Gamma_1^s, \dots, \Gamma_N^s\}$ as

$$\hat{\sigma}_{I \rightarrow J}(N) \equiv \frac{1}{T(N)} \sum_{i=1}^N \Delta S[\Gamma_i^s] \quad (15)$$

with $T(N)$ as the total elapsed time from the start of the observation until the end of the snippet Γ_N^s . This entropy production rate fluctuates with each realization as shown for $\tilde{K} \rightarrow \tilde{K}$ in Fig. 3(c). On the microscopic level, these fluctuations are due to different paths that all start with \tilde{K} and end with \tilde{K} . Although these paths cannot be resolved on the coarse-grained level, different paths typically lead to a different waiting time between the initial and final events. Therefore, the fluctuating duration of the snippets leads to a fluctuating entropy production. The entropy production rate converges towards its expectation value for a sufficient number of realizations as shown by the inset in Fig. 3(c).

G. Assumption on the microscopic level

The entropy production (7) for the coarse-grained trajectory Γ can be derived from a similar form on the microscopic level. We assume that the entropy production associated with a microscopic trajectory γ that starts with γ_0 and ends with γ_1 in a possibly time-dependent but not time-dependently driven system, like, e.g., a steady state or relaxation into it, is given by

$$\Delta s[\gamma] = \ln \frac{P(\gamma_0) \mathcal{P}[\gamma | \gamma_0]}{P(\gamma_1) \mathcal{P}[\tilde{\gamma} | \tilde{\gamma}_0]}. \quad (16)$$

Here, $\tilde{\gamma}_0 = \tilde{\gamma}_1$, i.e., the time-reversed trajectory $\tilde{\gamma}$ is initialized by the time-reversed final event of the original trajectory γ_1 . If the process is not stationary, the probabilities $P(\gamma_0)$ and $P(\gamma_1)$ depend on the initial and final times of the process, respectively. The identification (16) is well known to be correct for Markovian and overdamped Langevin dynamics as well as underdamped Langevin dynamics, as further detailed in Sec. IV A. Beyond these major system classes, Eq. (7) cannot be derived without further knowledge about the specific system and its energetics. However, we argue that even for such systems, Eq. (7) is a reasonable starting point if appropriate Markovian events can be identified, as the identification is physically correct for all verifiable classes of systems. Note that in the case of even observables we recover

$$\Delta s[\gamma] = \ln \frac{\mathcal{P}[\gamma]}{\mathcal{P}[\tilde{\gamma}]} \quad (17)$$

due to $\tilde{\gamma}_0 = \tilde{\gamma}_1 = \gamma_1$. We discuss the suggested relationship between Eq. (7) and the detailed fluctuation theorem (17) later in Sec. IV C.

At first glance unrelated, a comparison of the microscopic entropy production [Eq. (16)] to its coarse-grained counterpart [Eq. (7)] may stimulate the question whether a consistency relation of the form of Eq. (10) or Eq. (11) can be established beyond the setting considered above in which \mathcal{I} and \mathcal{J} are Markovian events on the microscopic level. More specifically, let us consider the case where the start and end of the microscopic trajectory map to the corresponding initial and

final events through a coarse graining of the form $\gamma_0 \mapsto \mathcal{I}$ and $\gamma_1 \mapsto \mathcal{J}$, respectively. As we prove in Appendix B, both Eq. (10) and Eq. (11) remain valid if both the microscopic and the coarse-grained level contain even variables only, but can be violated in the presence of odd variables. We will return to the discussion of odd variables and their peculiarities from a different angle in Sec. IV.

III. INFERENCE OF HIDDEN DRIVING

In a coarse-grained setup, the hidden part of a system is often not in equilibrium. It might even contain nonequilibrium processes, which do not directly drive any visible current or, more generally, any transition between two visible Markovian events. We refer to such processes as hidden driving, which arises if, e.g., the hidden part of a Markov network contains cycles with nonzero affinity.

In principle, the framework introduced in Sec. II allows for two strategies to localize and quantify nonequilibrium effects in a stationary state. First, we can use inequality (11) directly to bound the entropy production of microscopic trajectories that lead to particular snippets. Second, we can use the language of Markovian events to localize affinities \mathcal{A} of hidden driving, which can be regarded as the source of nonvanishing entropy production on the microscopic level. More formally, we can decompose the mean entropy production rate into contributions from individual cycles \mathcal{C} in the form [46,47]

$$\langle \sigma \rangle = \sum_{\mathcal{C}} j_{\mathcal{C}} \mathcal{A}_{\mathcal{C}} \quad (18)$$

in the steady state, where $j_{\mathcal{C}}$ is the expected number of completions of the cycle \mathcal{C} per unit time and $\mathcal{A}_{\mathcal{C}}$, the affinity of the cycle \mathcal{C} , is defined below in Sec. III B.

Both methods utilize the framework of Markovian events to derive quantitative bounds based on ratios of waiting-time distributions of the form of Eq. (7), which in the simplest case without additional data \mathcal{O} can be rewritten as

$$\Delta S[I \xrightarrow{t} J] = \ln \frac{P(I) \psi_{I \rightarrow J}(t)}{P(J) \psi_{\tilde{J} \rightarrow \tilde{I}}(t)} \quad (19)$$

for two Markovian events I, J . With the identification as a coarse-grained entropy production (7), the bound (11) provides an entropy estimator for every I, J and each value of t , whose practical use is demonstrated in Sec. III A. We can extract even more information if expression (19) takes different values as a function of t for fixed I, J . We will detail in Sec. III B how differences in $\Delta S[I \xrightarrow{t} J]$ due to its t dependence can be used to bound the affinity $\mathcal{A}_{\mathcal{C}}$ of hidden cycles \mathcal{C} .

A. Localizing entropy production

The coarse-grained entropy production (19) grants access to information far beyond its total mean. Since inequality (11) holds true for any snippet Γ^s , averaging over some but not all Γ^s still leads to a lower bound on the corresponding microscopic entropy production. For example, we might be interested in the entropy production of short snippets with a duration below a certain threshold. Alternatively, we might

TABLE I. Localization of entropy production in space and time for the Markov network shown in Fig. 2(b) in its steady state. Each pair of entries corresponds to one of the bounds stated in Eq. (21) with the microscopic entropy production rate σ_{con} on the left-hand side and its coarse-grained analog $\hat{\sigma}_{\text{con}}$ on the right-hand side. Each condition selects a path $I \rightarrow J$, with $I, J \in \{K, L, \tilde{K}, \tilde{L}\}$, and selects whether the snippet exceeds the duration $t_0 = 1$ or not. Adding the colored numbers yields the microscopic and coarse-grained entropy production rate for paths of the form $\tilde{K} \rightarrow \tilde{K}$ shown by the blue and red dashed lines in Fig. 3(c), respectively. Summing over all numbers on the right-hand side yields the estimator $\langle \hat{\sigma} \rangle \simeq 1.7$ as a bound on the mean total entropy production rate $\langle \sigma \rangle \simeq 2.9$, which is the sum over all numbers on the left-hand side. These values are shown by the darker blue and red dashed lines in Fig. 3(c). The rates used for simulations and further numerical details are provided in Appendix D.

		First event								
		K		L		\tilde{K}		\tilde{L}		
		σ_{con}	$\hat{\sigma}_{\text{con}}$	σ_{con}	$\hat{\sigma}_{\text{con}}$	σ_{con}	$\hat{\sigma}_{\text{con}}$	σ_{con}	$\hat{\sigma}_{\text{con}}$	
Final event	$t \leq t_0$	K	-4.0×10^{-3}	-4.9×10^{-3}	-2.6×10^{-4}	-3.7×10^{-4}	1.4×10^{-1}	1.4×10^{-1}	3.2×10^{-3}	3.6×10^{-4}
		L	-5.4×10^{-3}	-8.1×10^{-3}	-7.4×10^{-4}	-8.9×10^{-4}	5.1×10^{-2}	3.7×10^{-2}	3.0×10^{-2}	2.4×10^{-2}
		\tilde{K}	-8.8×10^{-2}	-1.0×10^{-1}	-3.0×10^{-3}	-5.0×10^{-3}	3.7×10^{-1}	2.8×10^{-1}	2.3×10^{-1}	1.9×10^{-1}
		\tilde{L}	1.1×10^{-2}	1.6×10^{-4}	-7.2×10^{-2}	-7.2×10^{-2}	2.8×10^{-1}	2.4×10^{-1}	7.5×10^{-2}	5.5×10^{-2}
$t > t_0$		K	-1.4×10^{-3}	-5.7×10^{-3}	-4.3×10^{-4}	-8.4×10^{-4}	4.6×10^{-2}	2.2×10^{-2}	1.0×10^{-2}	3.8×10^{-4}
		L	2.5×10^{-3}	-4.4×10^{-3}	-9.5×10^{-5}	-8.9×10^{-4}	8.5×10^{-2}	4.3×10^{-2}	2.4×10^{-2}	8.0×10^{-3}
		\tilde{K}	2.6×10^{-2}	-3.4×10^{-2}	-9.0×10^{-4}	-7.3×10^{-3}	7.8×10^{-1}	4.2×10^{-1}	2.2×10^{-1}	8.9×10^{-2}
		\tilde{L}	3.1×10^{-2}	1.1×10^{-3}	-1.6×10^{-3}	-4.2×10^{-3}	5.0×10^{-1}	3.3×10^{-1}	1.4×10^{-1}	7.8×10^{-2}

compare the entropy production of snippets $I \rightarrow J$ for different events I, J . More formally, we can derive

$$\begin{aligned} \hat{\sigma}_{\text{con}} &\equiv \sum_{\Gamma^s|_{\text{con}}} \frac{1}{\langle t \rangle} \mathcal{P}[\Gamma^s] \Delta S[\Gamma^s] \\ &\leq \sum_{\Gamma^s|_{\text{con}}} \frac{1}{\langle t \rangle} \mathcal{P}[\Gamma^s] \langle \Delta S | \Gamma^s \rangle \equiv \sigma_{\text{con}} \end{aligned} \quad (20)$$

from inequality (11), where the index ‘‘con’’ denotes that only those snippets that fulfill a certain condition contribute to the respective entropy production rate. The conversion constant $1/\langle t \rangle$ designates the rate at which snippets occur and mediates between entropy production per snippet and entropy production rates, which are given per unit time. With Eq. (20) as a quantitative tool, we are able to resolve contributions due to, say, short snippets or snippets between particular events. This spatial and/or temporal ‘‘localization’’ of entropy production yields a more refined picture than the mean total entropy production rate, where such details are lost.

We use the example shown in Fig. 2(b) to demonstrate the localization aspect implied by Eq. (20) and the resulting bounds on the microscopic entropy production rate. In this case, we have access to four observed transitions, K, \tilde{K}, L , and \tilde{L} , as well as the time elapsed between two consecutive events. Hence, we can resolve the total entropy production rate into contributions from different possible paths $I \rightarrow J$. In addition, we distinguish whether the duration of this path exceeded a threshold t_0 or not. Such a coarse, binary classification of short and long snippets can be useful even in the case of poor waiting time statistics, where the time-series data do not suffice to sample the full waiting time distributions that would be required to apply the identification (7) and the bound (11) directly. In total, the spatial and temporal classification leads to the 32 cases shown in Table I. For each combination, we

show both sides of the inequality

$$\sigma_{I \rightarrow J, t \leq t_0} \geq \hat{\sigma}_{I \rightarrow J, t \leq t_0}, \quad (21)$$

where each of the operationally accessible quantities on the right provides a lower bound on the corresponding microscopic entropy production term on the left, which is obtained by averaging all trajectories that satisfy the respective conditions.

The quantity $\hat{\sigma}_{I \rightarrow J}(N)$ introduced in Eq. (15) to illustrate the fluctuating properties of the coarse-grained entropy production approaches $\hat{\sigma}_{I \rightarrow J}$ in the limit of $N \rightarrow \infty$. Accordingly, we identify the expectation value of $\hat{\sigma}_{I \rightarrow J}(N)$ indicated by the red dashed line in Fig. 3(c) as the sum of $\hat{\sigma}_{I \rightarrow J, t > t_0}$ and $\hat{\sigma}_{I \rightarrow J, t < t_0}$ highlighted in red in Table I. Analogous relations apply to the corresponding microscopic quantities.

The quantity $\hat{\sigma}_{I \rightarrow J}(N)$ introduced in Eq. (15) to illustrate the fluctuating properties of the coarse-grained entropy production approaches $\hat{\sigma}_{I \rightarrow J}$ in the limit of $N \rightarrow \infty$. Accordingly, we identify the expectation value of $\hat{\sigma}_{I \rightarrow J}(N)$ indicated by the red dashed line in Fig. 3(c) as the sum of $\hat{\sigma}_{I \rightarrow J, t > t_0}$ and $\hat{\sigma}_{I \rightarrow J, t < t_0}$ highlighted in red in Table I. Analogous relations apply to the corresponding microscopic quantities.

Adding all the numbers for σ_{con} and $\hat{\sigma}_{\text{con}}$ in Table I yields the mean total entropy production rate $\langle \sigma \rangle$ and its estimator $\langle \hat{\sigma} \rangle$ established in Ref. [22], respectively. This example illustrates in which sense the localized coarse-grained entropy production (rate) allows us to infer much more detailed information than a single bound on its mean while, importantly, utilizing the same observables and waiting-time statistics.

The quality of estimator (20) varies depending on the condition, which becomes apparent when comparing different pairs of microscopic and corresponding coarse-grained entropy production in Table I. Consequently, the ratio of $\hat{\sigma}_{\text{con}}$ to $\langle \hat{\sigma} \rangle$ holds no implications on the corresponding microscopic ratio. Our method provides lower bounds on the entropy productions that are due to snippets of some particular type but not on their relative share of total entropy production.

B. Driving affinities

In this section, we describe how our framework can be used to detect hidden driven cycles and to bound the corresponding affinities from below. We assume an underlying Markov network in a stationary state, which is necessary to have a

well-defined notion of a cycle affinity of the form

$$\mathcal{A}_C = \sum_{(ij) \in C} \ln \frac{k_{ij}}{k_{ji}}, \quad (22)$$

where the sum runs over all transitions (ij) that point towards the same direction within a cycle C . The rate with which a transition (ij) occurs if the system is in state i is denoted by k_{ij} . For now, we consider snippets of the form

$$\Gamma^s : I \xrightarrow{t} J, \quad (23)$$

and postpone the discussion of additional non-Markovian information \mathcal{O} . We introduce the quantity

$$\Delta a_{I \rightarrow J} \equiv \sup_t \Delta S[I \xrightarrow{t} J] - \inf_t \Delta S[I \xrightarrow{t} J], \quad (24)$$

which allows us to bound the largest affinity of all cycles C hidden between I and J via

$$\max_C |\mathcal{A}_C| \geq \Delta a_{I \rightarrow J}, \quad (25)$$

as proved in Appendix C. This bound becomes more informative and therefore tighter whenever it is possible to distinguish between different microscopic paths that realize $I \xrightarrow{t} J$ based on the duration t . This affinity bound is related to similar bounds obtained independently in a recent work, which are formulated for logarithmic ratios of propagators rather than waiting time distributions [48].

We demonstrate a potential biochemical application of bound (25), which illustrates a method to infer cycle affinities in systems that are not directly observable. As an example, we consider the toy model shown in Fig. 4(a). We assume that we cannot measure any of the states that contribute to the cycle driving the system out of equilibrium. This remains true even after introducing an additional chemical species that is specifically designed to bind to the system in the fashion described in Fig. 4(a). However, this procedure allows to infer the chemical affinity of the driving cycle while remaining agnostic about states or transitions of the original system.

In Fig. 4(c) we present the results of the affinity estimation for the network shown in Fig. 4(b). We introduce the quantity

$$a_{I \rightarrow J}(t) = \ln \frac{\psi_{I \rightarrow J}(t)}{\psi_{\tilde{J} \rightarrow \tilde{I}}(t)}, \quad (26)$$

which is sufficient to determine $\Delta a_{I \rightarrow J}$ from Eq. (24) through

$$\Delta a_{I \rightarrow J} = \sup_t a_{I \rightarrow J}(t) - \inf_t a_{I \rightarrow J}(t) \quad (27)$$

since the probabilities $P(I)$ and $P(J)$ do not depend on the duration of the snippet t . In the present case with $I = 1$ and $J = 6$, the estimation yields $\Delta a_{1 \rightarrow 6} \simeq 3.3$ compared to the real cycle affinity of $\mathcal{A} \simeq 4.8$. Note that although this example relies on a unicyclic toy model, the same procedure can be applied to more complex systems, which then leads to a bound on the hidden cycle with the highest affinity.

We now give a heuristic explanation why a quantity of the form $\Delta a_{I \rightarrow J}$ results in an estimator for affinities rather than for entropy production as one might expect naively. We consider a snippet from state 1 to state 6 in Fig. 4(b) and assume that the cycle $C = (23452)$ has nonvanishing affinity. In this case, different microscopic paths lead to different entropy production,

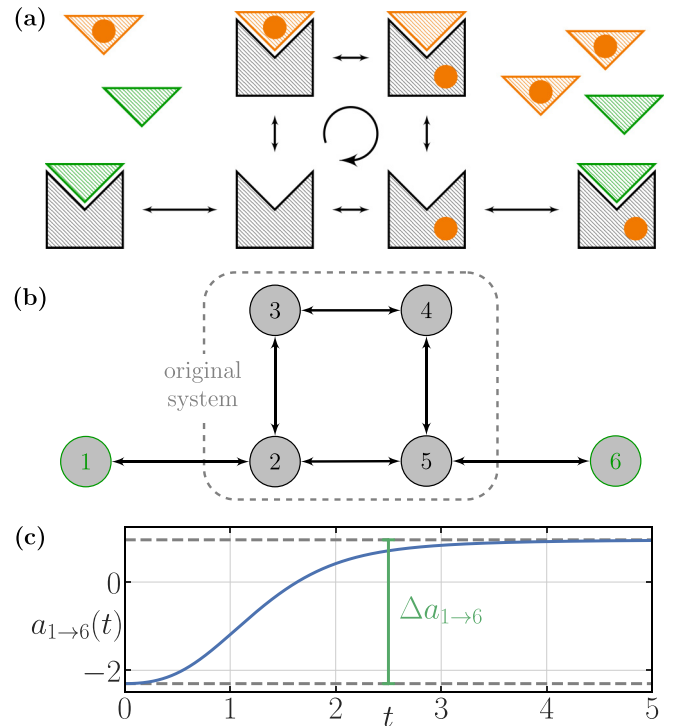


FIG. 4. (a) Toy model for the experimental inference of the affinity in a chemically driven system. We imagine a system in a solution of fuel-carrying molecules, similar to systems driven by the hydrolysis of ATP. The original system has four states, states 2 to 5, which are interconnected by the following four steps: the binding and unbinding of the molecule carrying the fuel, (23) and (45), respectively, the consumption of the fuel (52), and an intermediate step (34). For all of these steps, the reverse is also possible in accordance with the condition of thermodynamic consistency, which makes the transitions bidirectional. The green triangles represent an additional chemical species, which may bind to the system if it is not occupied by a fuel-carrying molecule, i.e., if the system is in state 2 or 5. Its binding prevents any further steps along the cycle leading to the two additional states 1 and 6. (b) The network corresponding to the system shown in (a). We assume that only states 1 and 6 can be observed. (c) Affinity estimation for the network shown in (b) leading to $\Delta a_{1 \rightarrow 6} \simeq 3.3$. The rates used for simulations and further numerical details are provided in Appendix D.

because they may include the cycle or not. Since on average shorter paths tend to avoid the cycle, the cycle manifests as a nontrivial time dependence in $\Delta S[I \xrightarrow{t} J]$. We might try to interpret Eq. (24) as a difference between averaged entropy productions of possible paths or, equivalently, as the averaged entropy production of the loop obtained by following one path forward and the other in reverse. However, it is then not obvious how to formulate a bound on this quantity, because in principle a microscopic path can contain the cycle C arbitrarily often, especially if C is strongly driven. Instead, the derivation of Eq. (25) does not rely on interpreting Eq. (24) as entropy production, but introduces a dual dynamics that uses an involution \mathcal{R} different to the time-reversal operation \mathcal{T} . As further detailed in Appendix C, the cycle-based methods to construct \mathcal{R} result in an interpretation of Eq. (24) as a quantity related to a cycle affinity instead of an entropy production.

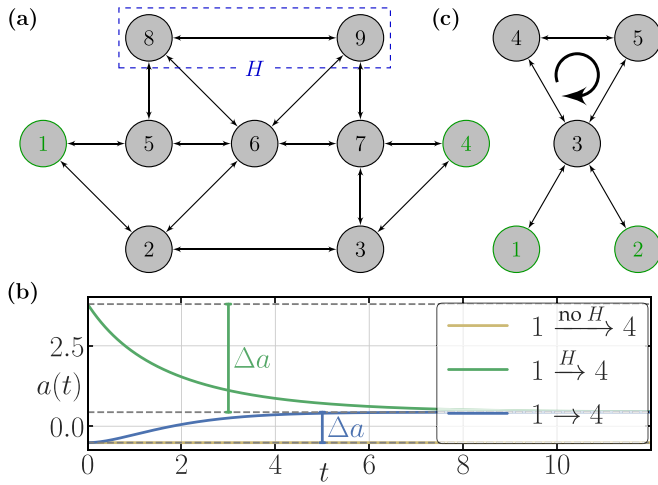


FIG. 5. (a) Markov network with nine states. We assume that only states 1 and 4 and the compound state H , consisting of states 8 and 9, can be observed. (b) Affinity estimation for the network shown in (a). The yellow line shows $a(t) \simeq -0.51$ independent of t for snippets $1 \xrightarrow{\text{no } H} 4$ that do not pass H . The green line shows $a(t)$ for snippets $1 \xrightarrow{H} 4$ that pass H at least once, which leads to $\Delta a \simeq 3.4$. For the blue line, the information about visiting H is discarded, i.e., both aforementioned types of snippets are included but not distinguished, which leads to $\Delta a \simeq 0.9$. The largest real cycle affinity in this network is $\mathcal{A} \simeq 7.8$. The rates used for simulations and further numerical details are provided in Appendix D. (c) Markov network with five states. We assume that only states 1 and 2 can be observed. The cycle $3 \rightarrow 4 \rightarrow 5 \rightarrow 3$ is driven in a clockwise direction.

Moreover, the derivation of bound (25) shows that additional observables besides I, J , and the time in between can be utilized as well if an additional consistency condition is satisfied. The proof primarily relies on constructing a suitable involution \mathcal{R} , which is referred to as partial [48,49] or mathematical [38] reversal \mathcal{R} and has to be indistinguishable from the true, physical time reversal for the given coarse graining. This condition has to be met also after introducing additional observables. In our case, \mathcal{R} acts like the true time-reversal operation on some parts of the trajectory while leaving other parts unchanged. Thus, any additional observables need to be even under time reversal. In particular, we cannot use waiting times between events for data \mathcal{O} in general, except for the duration of the snippet t .

An example for eligible further information is to include whether or not a compound state was visited during the snippet without including the time of the event. Including such additional information generally leads to an improvement of bound (25) and allows us to further localize the hidden driving. We illustrate this procedure on the example network shown in Fig. 5(a) where we observe the states 1 and 4 as well as the lumped state H . If we discard the information concerning H , we obtain an estimate for the affinity in a similar way as for the model illustrated in Fig. 4, as shown by the blue line in Fig. 5(b). When additionally observing H , we are able to extract two bounds. The first one applies to all cycles between 1 and 4 that do contain H , whereas the second one applies to all cycles between 1 and 4 that do not

contain H , shown by the green and yellow lines, respectively. We are able to correctly identify that there is no hidden driving outside of H and its connecting edges while also improving on the affinity estimator that does not discern whether H has been visited or not.

Finally we mention a case in which Eq. (24) fails to detect hidden driving, i.e., $\Delta a = 0$ despite $\mathcal{A} \neq 0$. If the driven cycle is connected to the remaining network only through a single state as shown in the example of Fig. 5(c), then its affinity does not result in a time-dependent $a(t)$. Put more generally, if a cycle can be located inside a compound state with direction-time independence [50,51] for all transitions to and from it, we are not able to infer its irreversibility from observables located entirely outside the compound state.

IV. INTRICACIES OF ODD VARIABLES

The identification of entropy production is particularly subtle in the case of odd observables since the observations I and \tilde{I} denote genuinely different objects. In the following, we examine two model classes based on such odd observables in detail.

A. Underdamped Langevin dynamics

For underdamped Langevin dynamics, the physically correct entropy production can be derived from the laws of stochastic energetics [52]. However, a detailed fluctuation theorem of the form of Eq. (17) does not hold [53–56]. In the following, we show and illustrate with some simple and well-understood examples that our approach is consistent with requirements for a physically meaningful entropy production in underdamped Langevin systems.

Consider an underdamped Brownian particle of mass M on a one-dimensional ring subject to a potential V and additionally to a nonconservative external force f in a nonequilibrium steady state. It is described by the Langevin equation

$$M\partial_t^2 x = -\gamma\partial_t x - \partial_x V(x) + f + M\xi(t), \quad (28)$$

in which ξ models uncorrelated Gaussian white noise

$$\langle \xi(t) \rangle = 0, \quad (29)$$

$$\langle \xi(t)\xi(t') \rangle = (2\gamma T/M^2)\delta(t - t'). \quad (30)$$

In this setup γ and T denote the friction constant, which is not to be confused with the microscopic trajectories, and the temperature in units of energy, i.e., $k_B = 1$, respectively.

Its entropy production has two contributions, one due to the stochastic entropy production ΔS_{st} and one associated with dissipation into the medium ΔS_m . First, we examine the entropy production along a trajectory Γ_a that starts with $I = (x_0, v_0)$ at time $T = 0$ and ends with $J = I$ after completing the cycle of length L at time T exactly once, as shown in Fig. 6(a) for $x_0 = -L/2 = L/2$. The stochastic contribution has to vanish since the initial and final states are identical. Therefore, we expect the total entropy production to be the cycle affinity $\mathcal{A} = fL$. Indeed, this is consistent with Eq. (7), which here becomes

$$\Delta S = \ln \frac{P(I)}{P(J)} + \ln \frac{\mathcal{P}[\Gamma|I]}{\mathcal{P}[\tilde{\Gamma}|\tilde{J}]} = \Delta S_{st} + \Delta S_m, \quad (31)$$

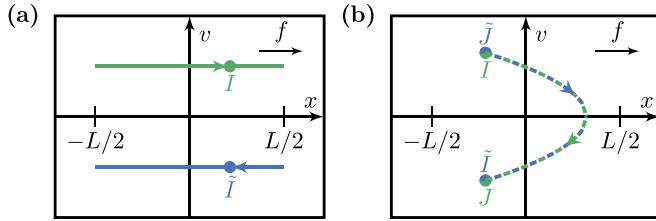


FIG. 6. Sketches of underdamped trajectories in phase space. (a) A trajectory Γ_a that starts and ends in I and completes the circle exactly once (green line) and its time reverse (blue line). (b) A trajectory Γ_b for which the velocity decreases linearly in time until the particle returns to its starting point (green curve). Its time reverse is identical to the forward trajectory (blue curve).

with $\Delta S_{st} = 0$ and $\Delta S_m = \int_0^T f \dot{x} dt = fL$.

In contrast, the tentative identification

$$\Delta S_{st}^{(i)} = \ln(P(I)/P(\tilde{I})), \quad (32)$$

for which $\Delta S^{(i)} \equiv \Delta S_m + \Delta S_{st}^{(i)}$ would obey a detailed fluctuation theorem of the form of Eq. (17), leads to $\Delta S_{st}^{(i)} \neq 0$ without a clear physical interpretation. First, this identification $\Delta S_{st}^{(i)}$ would not warrant the property of the stochastic entropy to purely depend on the state of the system. Second, the entropy production would not be additive. The sum of the entropy productions of two trajectories of the form shown in Fig. 6(a) would not be the same as the entropy production of the corresponding joint trajectory that completes the cycle twice.

A second identification of ΔS_{st} that reproduces the correct entropy production for the particular trajectory Γ_a would be

$$\Delta S_{st}^{(ii)} = \ln(P(\tilde{I})/P(\tilde{J})). \quad (33)$$

However, we can eliminate this possibility by considering a trajectory Γ_b from $I = (x_0, v_0)$ to $J = (x_0, -v_0)$ where the velocity initially is parallel to the nonconservative driving force and then linearly decreases with time as shown in Fig. 6(b). This trajectory is identical to its time reverse and, therefore, satisfies $\mathcal{P}[\Gamma|I] = \mathcal{P}[\tilde{\Gamma}|\tilde{J}]$ by construction. Due to the negative velocity, the final state of this trajectory is less probable than the initial one, which implies that the stochastic entropy should increase, as is indeed the case for

$$\Delta S_{st} = \ln \frac{P(I)}{P(J)} = \ln \frac{P(I)}{P(\tilde{I})}, \quad (34)$$

while the alternative $\Delta S_{st}^{(ii)}$ gives the wrong sign.

Finally, note that $-\ln(P(\tilde{I})/P(\tilde{J}))$ can be identified as the stochastic entropy production of the reverse trajectory in agreement with our formalism by applying Eq. (34) to $\tilde{\Gamma} = \tilde{J} \rightarrow \tilde{I}$.

B. Observed transitions

Transitions on a Markov network form a second class of systems with a description based on odd observables. We assume a system in a stationary state with only a few observable edges similar to the settings described in Refs. [23,38]. In this case, we can show that Eq. (7) is the correct identification of the entropy production through explicit calculations. We

consider a coarse-grained trajectory $\Gamma = I \rightarrow J$ that starts with transition I and ends with transition J . The corresponding microscopic trajectories share the form

$$\gamma = i \xrightarrow{I} j \rightarrow \dots \rightarrow k \xrightarrow{J} l, \quad (35)$$

where i, j and k, l are the Markov states associated with the transitions I and J , respectively. For the probabilities of these events as introduced in Sec. II C, we get the relations

$$P(I)/\langle t \rangle = p_i k_{ij} \quad \text{and} \quad P(J)/\langle t \rangle = p_k k_{kl}, \quad (36)$$

where p_i denotes the steady-state probability of microstate i . The right-hand sides are explicit expressions for the rates at which the respective transitions occur. For the left-hand sides, we write the rate for an observable transition I, J as the product of the total rate $1/\langle t \rangle$ that any observable transition occurs and the probability for that particular observable transition, $P(I)$ or $P(J)$, respectively. The normalization constant $1/\langle t \rangle$ disappears in ratios, e.g., of the form of Eq. (7), and denotes the inverse of the average length of a snippet [22]. The remaining path weights read

$$\mathcal{P}[I \rightarrow J|I] = \mathcal{P}[j \rightarrow k|j] k_{kl} \quad (37)$$

and

$$\mathcal{P}[\tilde{J} \rightarrow \tilde{I}|\tilde{J}] = \mathcal{P}[k \rightarrow j|k] k_{ji}. \quad (38)$$

The term $\mathcal{P}[j \rightarrow k|j]$ denotes the path weight for the trajectory starting immediately after entry into j until immediately before exiting k , given that the system starts in j . Inserting Eqs. (36), (37), and (38) into the coarse-grained entropy production [Eq. (7)] yields

$$\begin{aligned} \Delta S[\Gamma] &= \ln \frac{P(I)\mathcal{P}[I \rightarrow J|I]}{P(J)\mathcal{P}[\tilde{J} \rightarrow \tilde{I}|\tilde{J}]} = \ln \frac{p_i k_{ij} \mathcal{P}[j \rightarrow k|j] k_{kl}}{p_k k_{kl} \mathcal{P}[k \rightarrow j|k] k_{ji}} \\ &= \ln \frac{p_i k_{ij}}{p_j k_{ji}} + \ln \frac{\mathcal{P}[j \rightarrow k]}{\mathcal{P}[k \rightarrow j]}, \end{aligned} \quad (39)$$

where we identify $\Delta S[\Gamma]$ as the sum of the entropy production of the initial event I and the entropy production of the remaining part of the trajectory until immediately before the concluding event J . The final event is not included in the entropy production $\Delta S[\Gamma]$ in accordance with Sec. II E.

By analogy to the cases of Markov networks and underdamped Langevin dynamics, Eq. (39) suggests an identification of stochastic and medium entropy production in the form

$$\Delta S = \ln \frac{P(I)}{P(J)} + \ln \frac{\mathcal{P}[I \rightarrow J|I]}{\mathcal{P}[\tilde{J} \rightarrow \tilde{I}|\tilde{J}]} = \Delta S_{st} + \Delta S_m. \quad (40)$$

This identification of ΔS_{st} and ΔS_m must be clearly distinguished from the identification $\Delta s = \Delta s_{st} + \Delta s_m$ that can be made on the microscopic level for the Markov network [45]. We emphasize that the two identifications do not coincide even if the coarse graining retains the full entropy production, i.e., even if $\langle \Delta s \rangle = \langle \Delta S \rangle$, which is the case for, e.g., unicyclic Markov networks with a single observed transition [38]. In such a scenario, we have two physically sensible splittings into stochastic and medium entropy production. Thus, we interpret that the conception of ‘‘system’’ and ‘‘medium’’ can depend on the available information even if both descriptions apply to the same physical process on the microscopic level. For example, while stochastic entropy on the microscopic

level of the Markov network may change whenever the actual state i of the system changes, a corresponding quantity on the coarse-grained level updates when an observed transition I is registered.

Lastly, we point out that trying to transfer the concept of a fluctuating coarse-grained entropy production to lumped transitions, i.e., to events I that are triggered when one of several microscopic transitions occurs, causes two problems. First, an additivity property in the form of Eq. (8) is not valid in general because such events are not Markovian, i.e., do not satisfy Eq. (1). Second, in the general case we cannot establish a consistency condition of the form of Eqs. (10) or (11), which is demonstrated in a counterexample in Appendix B.

C. Discussion

The previous analysis of odd variables shows that even when considering stationary situations only, entropy production, in general, does not obey the detailed fluctuation theorem that applies to a Markovian dynamics [45]. Even if such an underlying Markovian description exists and Eq. (7) can be applied, we cannot expect a detailed fluctuation theorem of the same functional form as on the microscopic level, because the coarse-grained level involves different observables. However, validity is granted if all observables are even under time reversal, as seen by plugging $P(\tilde{\mathcal{J}}) = P(\mathcal{J})$ into Eq. (7). Thus, a refined understanding of the detailed fluctuation theorem may be as a symmetry associated with the special case of a description based on even observables in a Markovian dynamics rather than a general property of entropy production itself.

For underdamped Langevin dynamics in particular, entropy production is often expressed using some “modified” path weight for the reverse process [53,54,56], which leads to a formulation that appears similar to the detailed fluctuation theorem. However, this modified path weight and, therefore, the entire approach lack a clear physical interpretation. In light of the above insights regarding the detailed fluctuation theorem, it seems neither useful nor instructive to employ such a modified path weight.

An immediate consequence is that an expression of the form $\ln(\mathcal{P}[\gamma]/\mathcal{P}[\tilde{\gamma}])$ or $\ln(\mathcal{P}[\Gamma]/\mathcal{P}[\tilde{\Gamma}])$ cannot be regarded as a guiding principle for the identification of entropy production in arbitrary systems. For any system that on the underlying level fulfills the conditions described in Sec. II G, one should resort to the identification in Eq. (7). Beyond these, the identification of an entropy production requires knowledge of the underlying energetics and, additionally, considerations similar to the ones in Sec. IV A. The analysis of scenarios for which we understand the corresponding entropy production physically, such as in equilibrium or for simple trajectories, gives rise to consistency conditions that entropy production has to fulfill.

V. CONCLUDING PERSPECTIVE

In this work, we have established requirements to identify a fluctuating entropy production on a coarse-grained level. This concept offers practical advantages in resolving sources of irreversibility. Depending on the information available, we can quantify the contribution of particular snippets of a long

trajectory to the total entropy production and localize hidden driving with the aid of bounds on their affinity. As our identification is model-free, we put particular emphasis on the subtle case of odd variables.

Our framework does not rely on distinguishing slow and fast degrees of freedom. Such knowledge typically is hard to come by, particularly in the realistic case where some degrees of freedom are hidden. Thus, it is not necessary to identify a “correct fundamental layer,” i.e., a system comprising all slow-moving degrees of freedom which is surrounded by an environment that equilibrates on a faster timescale. Instead, the hidden parts of the system and the surrounding system are treated in the same way without making particular distinctions beforehand.

Finally, we point out that, in the general case, one should not expect to identify a physically meaningful entropy production on the coarse-grained level solely based on our approach in the absence of Markovian events, since our formalism necessarily requires a coarse-grained trajectory to start and end with a Markovian event. Applying Eq. (7) to arbitrary sections of a coarse-grained trajectory would generally imply a violation of the properties mentioned in Sec. II E, which would undermine the corresponding physical interpretation. In particular, the correspondence between microscopic and coarse-grained entropy production relies on the defining property of Markovian events.

We emphasize that, from a practical perspective, a model based on the identification of Markovian events entails milder assumptions than assuming that the underlying system obeys Markovian dynamics in the form of, e.g., a master equation. Rather than making assumptions about the entire system, for example, that every state is a Markov state, our framework only makes such assumptions within the visible part of the system. Conversely, if knowing the physical mechanisms of a model allows one to conclude that some observable states are Markovian, this is sufficient to apply our framework. Moreover, this framework allows one to formulate an operational criterion to falsify whether an event is Markovian based on coarse-grained data only [22].

The results of this paper allow for future research beyond the insights already demonstrated. As knowledge about the dynamics of the hidden parts of the system is not required, the improved flexibility of our framework should prove useful for applications across different model classes. Nevertheless, incorporating additional knowledge remains possible, as demonstrated for the estimation of cycle affinities when supposing an underlying network of Markov states. In a realistic biochemical setup, cycle affinities might be constrained to integer multiples of, say, the free energy released in hydrolysis of one ATP. Thus, if some microscopic states or transitions can be observed directly, the established affinity bounds that are able to distinguish different pathways provide a qualitative tool to localize the ATP-driven cycles in the biochemical network.

We expect that the concept of spatially and temporally localized entropy estimation can be combined successfully with other related techniques. Inferring entropy production through waiting times in snippets provides a physical interpretation for the waiting time distributions that have received attention in stochastic thermodynamics in different contexts. For example,

recently discovered thermodynamic bounds on waiting time distributions and correlation functions [30,31,33–35] might be combined with the notion of fluctuating entropy production to infer not only averages but full distributions of thermodynamic quantities.

In addition, our framework applies to systems in which the state of the system is known at some times, but the full dynamics remains inaccessible or unknown, which generalizes the paradigmatic cases of fully accessible Markov networks and overdamped Langevin equations. With this new perspective, we might speculate whether other concepts of stochastic thermodynamics beyond total entropy production like an identification of intrinsic and medium entropy production or stochastic energetics can also be extended to genuinely coarse-grained descriptions.

APPENDIX A: PROOF OF EQUALITY (10)

We consider a coarse-grained trajectory Γ , which starts with \mathcal{I} and ends with \mathcal{J} . Inserting the definition of the microscopic entropy production [Eq. (16)] into the mean on the right-hand side of Eq. (10) yields

$$\begin{aligned} \langle e^{-\Delta s} | \Gamma \rangle &= \sum_{\gamma \in \Gamma} \mathcal{P}[\gamma | \Gamma] \frac{P(\gamma_1) \mathcal{P}[\tilde{\gamma} | \tilde{\gamma}_1]}{P(\gamma_0) \mathcal{P}[\gamma | \gamma_0]} \\ &= \sum_{\gamma \in \Gamma} \mathcal{P}[\gamma | \Gamma] \frac{P(\mathcal{J}) \mathcal{P}[\tilde{\gamma} | \tilde{\mathcal{J}}]}{P(\mathcal{I}) \mathcal{P}[\gamma | \mathcal{I}]}. \end{aligned} \quad (\text{A1})$$

For the second equality we used that γ is initialized by the Markovian event \mathcal{I} , i.e., $\gamma_0 = \mathcal{I}$, and, likewise, $\gamma_1 = \mathcal{J}$. Note that $P(\gamma_0)$ does not necessarily correspond to the probability to observe the microscopic state of the trajectory at the time of the Markovian event.

Since the coarse graining defines a unique mapping $\gamma \mapsto \Gamma$, each microscopic trajectory γ implies its corresponding coarse-grained trajectory Γ . Thus, we can write $\mathcal{P}[\gamma | \Gamma] = P[\gamma] / \mathcal{P}[\Gamma] = P[\gamma] / (P(\mathcal{I}) \mathcal{P}[\Gamma | \mathcal{I}])$, which allows to calculate

$$\begin{aligned} &\sum_{\gamma \in \Gamma} \mathcal{P}[\gamma | \Gamma] \frac{P(\mathcal{J}) \mathcal{P}[\tilde{\gamma} | \tilde{\mathcal{J}}]}{P(\mathcal{I}) \mathcal{P}[\gamma | \mathcal{I}]} \\ &= \sum_{\gamma \in \Gamma} \frac{P[\gamma]}{P(\mathcal{I}) \mathcal{P}[\Gamma | \mathcal{I}]} \frac{P(\mathcal{J}) \mathcal{P}[\tilde{\gamma} | \tilde{\mathcal{J}}]}{P[\gamma]} \\ &= \frac{P(\mathcal{J})}{P(\mathcal{I}) \mathcal{P}[\Gamma | \mathcal{I}]} \sum_{\gamma \in \Gamma} \mathcal{P}[\tilde{\gamma} | \tilde{\mathcal{J}}] = \frac{P(\mathcal{J}) \mathcal{P}[\tilde{\Gamma} | \tilde{\mathcal{J}}]}{P(\mathcal{I}) \mathcal{P}[\Gamma | \mathcal{I}]} = e^{-\Delta s | \Gamma}. \end{aligned} \quad (\text{A2})$$

APPENDIX B: COUNTEREXAMPLE FOR COARSE-GRAINED EVENTS AND ODD VARIABLES

In Sec. II D, we define a snippet as a section of a coarse-grained trajectory between two events that are Markovian on the microscopic level. It is sensible to ask whether the results presented in Sec. II E remain valid if the condition of Markovianity on the microscopic level, i.e., $\gamma_0 = \mathcal{I}$ and $\gamma_1 = \mathcal{J}$, is relaxed. In this section, we explore this possibility by making the weaker assumption that the coarse graining that

maps $\gamma \mapsto \Gamma$ also maps the initial and final events of γ onto those of Γ in the form $\gamma_0 \mapsto \mathcal{I}$ and $\gamma_1 \mapsto \mathcal{J}$, respectively. Trying to compare $\langle e^{-\Delta s} | \Gamma \rangle$ and $e^{-\Delta s | \Gamma}$ following the same steps as in Eqs. (A1) and (A2) leads us to

$$\langle e^{-\Delta s} | \Gamma \rangle = \sum_{\gamma \in \Gamma} \mathcal{P}[\gamma | \Gamma] \frac{P(\mathcal{J}) \mathcal{P}[\tilde{\gamma} | \tilde{\gamma}_1] P(\gamma_1 | \mathcal{J})}{P(\mathcal{I}) \mathcal{P}[\gamma | \gamma_0] P(\gamma_0 | \mathcal{I})} \quad (\text{B1})$$

and

$$e^{-\Delta s | \Gamma} = \sum_{\gamma \in \Gamma} \mathcal{P}[\gamma | \Gamma] \frac{P(\mathcal{J}) \mathcal{P}[\tilde{\gamma} | \tilde{\mathcal{J}}]}{P(\mathcal{I}) \mathcal{P}[\gamma | \mathcal{I}]}, \quad (\text{B2})$$

respectively. Although the calculations remain basically unchanged, the numerators in expressions (B1) and (B2) differ by a term of the form

$$e^\delta \equiv \frac{P(\gamma_1 | \mathcal{J})}{P(\tilde{\gamma}_1 | \tilde{\mathcal{J}})}. \quad (\text{B3})$$

Thus, even if the initial and final events of a snippet are defined on the coarse-grained level, we can use $\mathcal{P}[\tilde{\gamma} | \tilde{\gamma}_1] P(\tilde{\gamma}_1 | \tilde{\mathcal{J}}) = \mathcal{P}[\tilde{\gamma} | \tilde{\mathcal{J}}]$ to establish Eq. (10) provided $\delta = 0$ vanishes identically. In addition to the model classes in which no coarse graining happens at the Markovian events, i.e., $\gamma_1 = \mathcal{J}$, model classes in which any conceivable γ_1 and \mathcal{J} are even under time reversal also satisfy this condition $\delta = 0$. For example, this is the case when considering lumped states in Markov networks, since residence in such states is even under time reversal.

However, in the presence of odd variables, we get $\delta \neq 0$ in the general case. As an example, consider a unicyclic Markov network that consists of three interconnected states 1, 2, and 3 and is in the steady state. We assume that we observe transitions in the form $I = (31)$, $\tilde{I} = (13)$ and $J = \{(12), (23)\}$, $\tilde{J} = \{(21), (32)\}$ which are odd under time reversal, although the underlying microscopic dynamics is not. Due to the assumption that we cannot discern the transitions $1 \rightarrow 2$ and $2 \rightarrow 3$ or their corresponding reverses, J and its time reverse \tilde{J} do not satisfy the defining property of Markovian events, whereas I and \tilde{I} are Markovian events on the microscopic level in accordance with Sec. IV B.

Denoting the steady-state distribution by p_i and the transition rates by k_{ij} , we can calculate the rate with which one of the four events $I, J, \tilde{I}, \tilde{J}$ occurs as $1/\langle t \rangle = \sum_{ij} p_i k_{ij}$. We consider a microscopic trajectory starting with a transition $\gamma_0 = (31)$ at time zero and ending with a subsequent transition $\gamma_1 = (12)$ at time t , which is coarse grained into $\Gamma = I \xrightarrow{t} J$ with time reverse $\tilde{\Gamma} = \tilde{J} \xrightarrow{t} \tilde{I}$. Since Γ is only comprised of this single microscopic trajectory, calculating the average

$$\langle e^{-\Delta s} | \Gamma \rangle = e^{-\Delta s} = \frac{p_1 k_{13}}{p_3 k_{31}} \quad (\text{B4})$$

is trivial and includes the microscopic entropy production of the transition I but not of J as described in Sec. II E. We use the explicit expressions

$$\begin{aligned} P(I)/\langle t \rangle &= p_3 k_{31}, \quad \mathcal{P}[\Gamma | I] = e^{-(k_{12} + k_{13})t} k_{12}, \\ P(J)/\langle t \rangle &= p_1 k_{12} + p_2 k_{23}, \quad \mathcal{P}[\tilde{\Gamma} | \tilde{J}] = P((21) | \tilde{J}) \mathcal{P}[\tilde{\Gamma} | (21)] \\ &= \frac{p_2 k_{21}}{p_2 k_{21} + p_3 k_{32}} e^{-(k_{12} + k_{13})t} k_{13}, \end{aligned} \quad (\text{B5})$$

to compare the coarse-grained and microscopic entropy production terms

$$e^{-\Delta S[\Gamma]} = \frac{P(J)\mathcal{P}[\tilde{\Gamma}|\tilde{J}]}{P(I)\mathcal{P}[\Gamma|I]} = \frac{p_1 k_{13}}{p_3 k_{31}} \frac{p_2 k_{21}}{p_2 k_{21} + p_3 k_{32}} \frac{p_1 k_{12} + p_2 k_{23}}{p_1 k_{12}} = \left\langle e^{-\Delta s} \frac{P(\tilde{\gamma}_1|\tilde{\mathcal{J}})}{P(\gamma_1|\mathcal{J})} \middle| \Gamma \right\rangle = \langle e^{-\Delta s - \delta} | \Gamma \rangle. \quad (\text{B6})$$

This counterexample shows that Markovian events on the microscopic level are required to establish a relation of the form of Eq. (10) if odd variables are involved. We also note that the term δ can have either sign, so that the implied inequality (11) can also be violated if the condition of Markovianity on the microscopic level is not met. As an explicit example, consider $k_{12} = k_{21} = k_{31} = k_{13} = 1$. If the remaining rates are chosen as $k_{23} = 1$ and $k_{32} = 2$, we calculate $p_1 = 1/3$, $p_2 = 5/12$, $p_3 = 1/4$, and $\delta \simeq -0.022$, whereas for $k_{32} = 1$ and $k_{23} = 2$ we obtain $p_1 = 1/3$, $p_2 = 1/4$, $p_3 = 5/12$, and $\delta \simeq 0.065$.

APPENDIX C: PROOF OF THE AFFINITY BOUND (25)

For the proof of the bound (25), we assume an underlying Markov network in a stationary state, some coarse graining \mathcal{C} , and a time-reversal operation \mathcal{T} with $\mathcal{T}\gamma = \tilde{\gamma}$, which is an involution. We consider a second involution \mathcal{R} , which has the property that it is not distinguishable from the time reversal \mathcal{T} under coarse graining, i.e.,

$$\begin{array}{ccc} \gamma & \xrightarrow{\mathcal{T}} & \tilde{\gamma} \\ \downarrow \mathcal{R} & & \downarrow \mathcal{C} \\ \mathcal{R}\gamma & \xrightarrow{\mathcal{C}} & \tilde{\Gamma} \end{array} \quad (\text{C1})$$

Since additionally \mathcal{R} is a bijection, we conclude

$$\mathcal{P}[\tilde{\Gamma}|\tilde{J}] = \sum_{\gamma \in \Gamma} \mathcal{P}[\tilde{\gamma}|\tilde{J}] = \sum_{\gamma \in \Gamma} \mathcal{P}[\mathcal{R}\gamma|\tilde{J}]. \quad (\text{C2})$$

For a trajectory γ that starts with the Markovian event I and ends with the Markovian event J , we define

$$A[\gamma] \equiv \ln \frac{\mathcal{P}[\gamma|I]}{\mathcal{P}[\mathcal{R}\gamma|\tilde{J}]}. \quad (\text{C3})$$

Note that \tilde{J} necessarily is the initial event of $\mathcal{R}\gamma$ due to the relation (C1). Using the definition (C3), we rewrite

$$\mathcal{P}[\Gamma|I] = \sum_{\gamma \in \Gamma} \mathcal{P}[\gamma|I] = \sum_{\gamma \in \Gamma} \mathcal{P}[\mathcal{R}\gamma|\tilde{J}] e^{A[\gamma]}. \quad (\text{C4})$$

Combining Eqs. (C2) and (C4), we find

$$\frac{\mathcal{P}[\Gamma|I]}{\mathcal{P}[\tilde{\Gamma}|\tilde{J}]} = \frac{\sum_{\gamma \in \Gamma} \mathcal{P}[\mathcal{R}\gamma|\tilde{J}] e^{A[\gamma]}}{\sum_{\gamma \in \Gamma} \mathcal{P}[\mathcal{R}\gamma|\tilde{J}]} = \langle e^{A[\gamma]} \rangle_{\text{aux}}, \quad (\text{C5})$$

where we identify the expression in the middle as a mean with respect to some auxiliary probability measure. This relation implies

$$\inf_{\gamma \in \Gamma} e^{A[\gamma]} \leq \langle e^{A[\gamma]} \rangle_{\text{aux}} \leq \sup_{\gamma \in \Gamma} e^{A[\gamma]}. \quad (\text{C6})$$

Inserting Eq. (C5) into Eq. (C6) yields

$$\inf_{\gamma \in \Gamma} A[\gamma] \leq \ln \frac{\mathcal{P}[\Gamma|I]}{\mathcal{P}[\tilde{\Gamma}|\tilde{J}]} \leq \sup_{\gamma \in \Gamma} A[\gamma], \quad (\text{C7})$$

where we also use the monotonicity of the logarithm. Inequalities (C7) hold for any coarse-grained trajectory Γ . By considering all trajectories that start in I and end in J , denoted symbolically as $\gamma|I \rightarrow J$, we obtain

$$\begin{aligned} & \sup_{\gamma|I \rightarrow J} A[\gamma] - \inf_{\gamma|I \rightarrow J} A[\gamma] \\ & \geq \sup_{\Gamma|I \rightarrow J} \ln \frac{\mathcal{P}[\Gamma|I]}{\mathcal{P}[\tilde{\Gamma}|\tilde{J}]} - \inf_{\Gamma|I \rightarrow J} \ln \frac{\mathcal{P}[\Gamma|I]}{\mathcal{P}[\tilde{\Gamma}|\tilde{J}]} \end{aligned} \quad (\text{C8})$$

Since the initial and final events are fixed, the probabilities $P(I)$ and $P(J)$ are identical for all these trajectories, so that the duration of the snippet becomes the only remaining variable, which finally results in

$$\begin{aligned} & \sup_{\gamma|I \rightarrow J} A[\gamma] - \inf_{\gamma|I \rightarrow J} A[\gamma] \\ & \geq \sup_t \ln \frac{P(I)\mathcal{P}[\Gamma|I]}{P(J)\mathcal{P}[\tilde{\Gamma}|\tilde{J}]} - \inf_t \ln \frac{P(I)\mathcal{P}[\Gamma|I]}{P(J)\mathcal{P}[\tilde{\Gamma}|\tilde{J}]} \\ & = \sup_t \Delta S[I \xrightarrow{t} J] - \inf_t \Delta S[I \xrightarrow{t} J]. \end{aligned} \quad (\text{C9})$$

To extract a physically meaningful bound from inequality (C9), we need to explicitly construct \mathcal{R} , where we follow an algorithm similar to Ref. [38]. Consider the microscopic trajectory on the Markov network $\gamma = I \rightarrow k \rightarrow \dots \rightarrow l \rightarrow J = Ik \dots lJ$, where I and J are the Markovian events, in this case states or transitions, and $k \dots l$ the remaining Markov states visited in between. To construct $\mathcal{R}\gamma$, we perform the following steps:

(1) Separate the trajectory into closed loops and the remaining parts. Starting after I and stopping before J , if a state occurs more than once, we identify a closed loop as the intermediate section between the first and last appearance including the states at the beginning and end of the loop,

$$(\dots axb \dots cxd \dots) \mapsto (\dots a)(xb \dots cx)(d \dots). \quad (\text{C10})$$

It is not necessary to identify loops within loops.

(2) Reverse the order of sections, i.e.,

$$(a \dots b)(cd \dots ec)(f \dots g) \mapsto (f \dots g)(cd \dots ec)(a \dots b). \quad (\text{C11})$$

(3) Reverse the order of states within the sections that do not form a closed loop. These are the sections with differing initial and final states, i.e.,

$$(f \dots g)(cd \dots ec)(a \dots b) \mapsto (g \dots f)(cd \dots ec)(b \dots a). \quad (\text{C12})$$

(4) Reverse I and J , i.e.,

$$I \mapsto \tilde{I}, J \mapsto \tilde{J}. \quad (\text{C13})$$

(5) Merge the resulting section.

Note that the residence times in each state are not affected by \mathcal{R} . This involution satisfies $\mathcal{C}\mathcal{R}\gamma = \tilde{\Gamma}$ since any microscopic trajectory $Ik \dots lJ$ maps to the coarse-grained

trajectory $I \rightarrow J$ without any additional observables. The involution \mathcal{R} treats these initial and final events I and J in the same way as the original time-reversal operation.

We define γ^{trim} as the trimmed trajectory that results from removing the closed loops of γ in the form of

$$\gamma = abcdecfg \Rightarrow \gamma^{\text{trim}} = abcfg, \quad (\text{C14})$$

where the loops are identified in the same way as in step 1. With this explicit definition of \mathcal{R} , we identify

$$A[\gamma] = A[\gamma^{\text{trim}}] + C(I, J) \quad (\text{C15})$$

with the affinity

$$\mathcal{A}[\gamma] \equiv \sum_{(ij) \in \gamma} \ln \frac{k_{ij}}{k_{ji}} = \ln \frac{\mathcal{P}[\gamma|\gamma_0]}{\mathcal{P}[\tilde{\gamma}|\tilde{\gamma}_0]}, \quad (\text{C16})$$

where the sum runs over all transitions in γ . $C(I, J)$ denotes a boundary term, which exclusively depends on I and J and vanishes identically if I and J denote Markov states, but in the general case can be nonzero. For example, if $I = (ij)$ and $J = (mn)$ denote transitions (and the full trajectory has the sequence of visited states $ijk \cdots lmn$), the term $A[\gamma]$ as defined in Eq. (C3) differs from $A[\gamma^{\text{trim}}]$ due to the conditioning on I and \tilde{J} in the numerator and denominator, respectively. In this case, an explicit calculation establishes $\mathcal{A}[\gamma^{\text{trim}}] = A[\gamma] + \ln(k_{ij}/k_{nm})$. Hence, the resulting boundary term $C(I, J)$ is fully determined by I and J and independent of the microscopic details of γ .

For the reasoning of the proof, an explicit form of the term $C(I, J)$ is not required, as this term vanishes after taking differences in Eq. (C9). We can then identify the resulting terms as an extremal cycle affinity, i.e.,

$$\sup_{\gamma|I \rightarrow J} A[\gamma] - \inf_{\gamma|\tilde{I} \rightarrow \tilde{J}} A[\gamma] = \max_{\mathcal{C}} \mathcal{A}_{\mathcal{C}}, \quad (\text{C17})$$

where the maximum runs over all cycles \mathcal{C} that can be obtained as a loop formed by going a trimmed path γ_1^{trim} from I to J followed by going a trimmed path $\mathcal{T}\gamma_2^{\text{trim}}$ from \tilde{J} back to \tilde{I} . Symbolically, such cycles \mathcal{C} can be written as

$\gamma_1^{\text{trim}} \rightarrow \mathcal{T}\gamma_2^{\text{trim}} = \gamma_1^{\text{trim}} \rightarrow \tilde{\gamma}_2^{\text{trim}}$. Note that each affinity $\mathcal{A}_{\mathcal{C}}$ occurs with either sign, so that the maximum selects the cycle affinity with the highest absolute value. By inserting Eq. (C17) into bound (C9), we finally arrive at

$$\max_{\mathcal{C}} \mathcal{A}_{\mathcal{C}} \geq \sup_I \Delta S[I \xrightarrow{t} J] - \inf_{\tilde{I}} \Delta S[\tilde{I} \xrightarrow{t} \tilde{J}], \quad (\text{C18})$$

which is Eq. (25) in the main text.

APPENDIX D: NUMERICAL DETAILS

For the illustrations in Secs. II F, III A, and III B we rely on the numerical computation of coarse-grained path weights of the form $P(I)\mathcal{P}[I \rightarrow J|I]$. The first term, $P(I)$, can be calculated from the solution of the corresponding master equation. The second term, $\mathcal{P}[I \rightarrow J|I]$, is computed by solving the corresponding absorbing master equation as described in Ref. [57] and detailed further in the Appendix of Ref. [38].

For Fig. 3, we first use this method of absorbing master equations to compute the coarse-grained path weights. We then simulate individual trajectories on the corresponding underlying Markov network to which we apply the coarse graining and calculate the coarse-grained entropy production using these path weights in Eq. (7).

The rates for the network shown in Fig. 2(b) are $k_{12} = 0.6$, $k_{21} = 2$, $k_{23} = 2.1$, $k_{32} = 5$, $k_{26} = 1.4$, $k_{62} = 2$, $k_{34} = 0.3$, $k_{43} = 3$, $k_{35} = 0.9$, $k_{53} = 4.3$, $k_{36} = 1$, $k_{63} = 1.6$, $k_{45} = 0.5$, $k_{54} = 2$, $k_{56} = 0.8$, $k_{65} = 4$, $k_{61} = 1.8$, and $k_{16} = 3$.

The rates for the network shown in Fig. 4(b) are $k_{12} = 2.5$, $k_{21} = 2.5$, $k_{23} = 0.7$, $k_{25} = 0.1$, $k_{32} = 0.3$, $k_{34} = 0.7$, $k_{43} = 0.3$, $k_{45} = 0.7$, $k_{52} = 1$, $k_{54} = 0.3$, $k_{56} = 2.5$, and $k_{65} = 2.5$.

The rates for the network shown in Fig. 5(a) are $k_{12} = 1$, $k_{15} = 1.5$, $k_{21} = 1$, $k_{23} = 1$, $k_{26} = 0.5$, $k_{32} = 1$, $k_{34} = 1$, $k_{37} = 0.5$, $k_{43} = 1$, $k_{47} = 0.5$, $k_{51} = 1.5$, $k_{56} = 0.5$, $k_{58} = 0.5$, $k_{62} = 0.5$, $k_{65} = 0.5$, $k_{67} = 0.5$, $k_{68} = 0.1$, $k_{69} = 0.5$, $k_{73} = 0.5$, $k_{74} = 0.5$, $k_{76} = 0.5$, $k_{79} = 0.1$, $k_{85} = 0.1$, $k_{86} = 0.5$, $k_{89} = 3$, $k_{96} = 0.1$, $k_{97} = 2$, and $k_{98} = 4$.

-
- [1] U. Seifert, Stochastic thermodynamics, fluctuation theorems, and molecular machines, *Rep. Prog. Phys.* **75**, 126001 (2012).
 - [2] C. van den Broeck and M. Esposito, Ensemble and trajectory thermodynamics: A brief introduction, *Physica A* **418**, 6 (2015).
 - [3] C. Jarzynski, Nonequilibrium equality for free energy differences, *Phys. Rev. Lett.* **78**, 2690 (1997).
 - [4] G. E. Crooks, Nonequilibrium measurements of free energy differences for microscopically reversible Markovian systems, *J. Stat. Phys.* **90**, 1481 (1998).
 - [5] C. Jarzynski, Equalities and inequalities: Irreversibility and the second law of thermodynamics at the nanoscale, *Annu. Rev. Condens. Matter Phys.* **2**, 329 (2011).
 - [6] J. Kurchan, Fluctuation theorem for stochastic dynamics, *J. Phys. A: Math. Gen.* **31**, 3719 (1998).
 - [7] J. L. Lebowitz and H. Spohn, A Gallavotti-Cohen-type symmetry in the large deviation functional for stochastic dynamics, *J. Stat. Phys.* **95**, 333 (1999).
 - [8] G. E. Crooks, Entropy production fluctuation theorem and the nonequilibrium work relation for free energy differences, *Phys. Rev. E* **60**, 2721 (1999).
 - [9] G. E. Crooks, Path-ensemble averages in systems driven far from equilibrium, *Phys. Rev. E* **61**, 2361 (2000).
 - [10] M. Esposito and C. van den Broeck, Three detailed fluctuation theorems, *Phys. Rev. Lett.* **104**, 090601 (2010).
 - [11] T. Hatano and S.-i. Sasa, Steady-state thermodynamics of Langevin systems, *Phys. Rev. Lett.* **86**, 3463 (2001).
 - [12] T. Harada and S. I. Sasa, Equality connecting energy dissipation with a violation of the fluctuation-response relation, *Phys. Rev. Lett.* **95**, 130602 (2005).
 - [13] S. Ciliberto, Experiments in stochastic thermodynamics: Short history and perspectives, *Phys. Rev. X* **7**, 021051 (2017).
 - [14] U. Seifert, From stochastic thermodynamics to thermodynamic inference, *Annu. Rev. Condens. Matter Phys.* **10**, 171 (2019).

- [15] A. C. Barato and U. Seifert, Thermodynamic uncertainty relation for biomolecular processes, *Phys. Rev. Lett.* **114**, 158101 (2015).
- [16] T. R. Gingrich, J. M. Horowitz, N. Perunov, and J. L. England, Dissipation bounds all steady-state current fluctuations, *Phys. Rev. Lett.* **116**, 120601 (2016).
- [17] J. M. Horowitz and T. R. Gingrich, Thermodynamic uncertainty relations constrain non-equilibrium fluctuations, *Nat. Phys.* **16**, 15 (2020).
- [18] R. Kawai, J. M. R. Parrondo, and C. Van den Broeck, Dissipation: The phase-space perspective, *Phys. Rev. Lett.* **98**, 080602 (2007).
- [19] E. Roldan and J. M. R. Parrondo, Estimating dissipation from single stationary trajectories, *Phys. Rev. Lett.* **105**, 150607 (2010).
- [20] G. Bisker, M. Polettni, T. R. Gingrich, and J. M. Horowitz, Hierarchical bounds on entropy production inferred from partial information, *J. Stat. Mech.* (2017) 093210.
- [21] I. A. Martínez, G. Bisker, J. M. Horowitz, and J. M. R. Parrondo, Inferring broken detailed balance in the absence of observable currents, *Nat. Commun.* **10**, 3542 (2019).
- [22] J. van der Meer, J. Degünther, and U. Seifert, Time-resolved statistics of snippets as general framework for model-free entropy estimators, *Phys. Rev. Lett.* **130**, 257101 (2023).
- [23] P. E. Harunari, A. Dutta, M. Polettni, and E. Roldan, What to learn from a few visible transitions' statistics? *Phys. Rev. X* **12**, 041026 (2022).
- [24] U. Kapustin, A. Ghosal, and G. Bisker, Utilizing time-series measurements for entropy production estimation in partially observed systems, [arXiv:2212.13487](https://arxiv.org/abs/2212.13487) [Phys. Rev. Res. (to be published)].
- [25] N. Shiraishi, K. Funo, and K. Saito, Speed limit for classical stochastic processes, *Phys. Rev. Lett.* **121**, 070601 (2018).
- [26] S. Ito and A. Dechant, Stochastic time evolution, information geometry, and the Cramér-Rao bound, *Phys. Rev. X* **10**, 021056 (2020).
- [27] I. Neri, E. Roldán, and F. Jülicher, Statistics of infima and stopping times of entropy production and applications to active molecular processes, *Phys. Rev. X* **7**, 011019 (2017).
- [28] D. J. Skinner and J. Dunkel, Improved bounds on entropy production in living systems, *Proc. Natl. Acad. Sci. USA* **118**, e2024300118 (2021).
- [29] P. Pietzonka and F. Coghi, Thermodynamic cost for precision of general counting observables, [arXiv:2305.15392](https://arxiv.org/abs/2305.15392).
- [30] N. Ohga, S. Ito, and A. Kolchinsky, Thermodynamic bound on the asymmetry of cross-correlations, *Phys. Rev. Lett.* **131**, 077101 (2023).
- [31] N. Shiraishi, Entropy production limits all fluctuation oscillations, *Phys. Rev. E* **108**, L042103 (2023).
- [32] T. V. Vu, V. T. Vo, and K. Saito, Dissipation, quantum coherence, and asymmetry of finite-time cross-correlations, *Phys. Rev. Res.* **6**, 013273 (2024).
- [33] A. Dechant, Thermodynamic constraints on the power spectral density in and out of equilibrium, [arXiv:2306.00417](https://arxiv.org/abs/2306.00417).
- [34] A. Dechant, J. Garnier-Brun, and S.-i. Sasa, Thermodynamic bounds on correlation times, *Phys. Rev. Lett.* **131**, 167101 (2023).
- [35] A. Kolchinsky, N. Ohga, and S. Ito, Thermodynamic bound on spectral perturbations, with applications to oscillations and relaxation dynamics, *Phys. Rev. Res.* **6**, 013082 (2024).
- [36] X. Li and A. B. Kolomeisky, Mechanisms and topology determination of complex chemical and biological network systems from first-passage theoretical approach, *J. Chem. Phys.* **139**, 144106 (2013).
- [37] A. L. Thorneywork, J. Gladrow, Y. Qing, M. Rico-Pasto, F. Ritort, H. Bayley, A. B. Kolomeisky, and U. F. Keyser, Direct detection of molecular intermediates from first-passage times, *Sci. Adv.* **6**, eaaz4642 (2020).
- [38] J. van der Meer, B. Ertel, and U. Seifert, Thermodynamic inference in partially accessible Markov networks: A unifying perspective from transition-based waiting time distributions, *Phys. Rev. X* **12**, 031025 (2022).
- [39] M. Esposito, Stochastic thermodynamics under coarse-graining, *Phys. Rev. E* **85**, 041125 (2012).
- [40] D. Seifert, P. Sollich, and S. Klumpp, Coarse graining of biochemical systems described by discrete stochastic dynamics, *Phys. Rev. E* **102**, 062149 (2020).
- [41] D. Hartich and A. Godec, Violation of local detailed balance upon lumping despite a clear timescale separation, *Phys. Rev. Res.* **5**, L032017 (2023).
- [42] A. Godec and D. E. Makarov, Challenges in inferring the directionality of active molecular processes from single-molecule fluorescence resonance energy transfer trajectories, *J. Phys. Chem. Lett.* **14**, 49 (2023).
- [43] R. Elber, Milestoning: An efficient approach for atomically detailed simulations of kinetics in biophysics, *Annu. Rev. Biophys.* **49**, 69 (2020).
- [44] D. Hartich and A. Godec, Emergent memory and kinetic hysteresis in strongly driven networks, *Phys. Rev. X* **11**, 041047 (2021).
- [45] U. Seifert, Entropy production along a stochastic trajectory and an integral fluctuation theorem, *Phys. Rev. Lett.* **95**, 040602 (2005).
- [46] T. L. Hill, *Free Energy Transduction and Biochemical Cycle Kinetics*, 2nd ed. (Dover, Mineola, NY, 1989).
- [47] D. Jiang, M. Qian, and M.-P. Qian, *Mathematical Theory of Nonequilibrium Steady-States* (Springer-Verlag, Amsterdam, 2004).
- [48] S. Liang and S. Pigolotti, Thermodynamic bounds on time-reversal asymmetry, *Phys. Rev. E* **108**, L062101 (2023).
- [49] M. Polettni, G. Falasco, and M. Esposito, Tight uncertainty relations for cycle currents, *Phys. Rev. E* **106**, 064121 (2022).
- [50] H. Wang and H. Qian, On detailed balance and reversibility of semi-Markov processes and single-molecule enzyme kinetics, *J. Math. Phys.* **48**, 013303 (2007).
- [51] B. Ertel, J. van der Meer, and U. Seifert, Operationally accessible uncertainty relations for thermodynamically consistent semi-Markov processes, *Phys. Rev. E* **105**, 044113 (2022).
- [52] K. Sekimoto, *Stochastic Energetics* (Springer, Berlin, 2010).
- [53] R. E. Spinney and I. J. Ford, Nonequilibrium thermodynamics of stochastic systems with odd and even variables, *Phys. Rev. Lett.* **108**, 170603 (2012).
- [54] R. E. Spinney and I. J. Ford, Entropy production in full phase space for continuous stochastic dynamics, *Phys. Rev. E* **85**, 051113 (2012).

- [55] H. K. Lee, C. Kwon, and H. Park, Fluctuation theorems and entropy production with odd-parity variables, *Phys. Rev. Lett.* **110**, 050602 (2013).
- [56] L. P. Fischer, H.-M. Chun, and U. Seifert, Free diffusion bounds the precision of currents in underdamped dynamics, *Phys. Rev. E* **102**, 012120 (2020).
- [57] K. Sekimoto, Derivation of the first passage time distribution for Markovian process on discrete network, [arXiv:2110.02216](https://arxiv.org/abs/2110.02216).